Electrochimica Acta 105 (2013) 209–217

Contents lists available at SciVerse ScienceDirect

Electrochimica Acta

journal homepage: www.elsevier.com/locate/electacta

Mechanism and dissolution rates of anodic oxide films on silicon

D.Q. Liu, D.J. Blackwood *

Department of Materials Science and Engineering, National University of Singapore, Block E3A, 7 Engineering Drive 1, Singapore 117574, Singapore

ARTICLE INFO

Article history:
Received 25 December 2012
Received in revised form 1 April 2013
Accepted 2 April 2013
Available online 26 April 2013

Keywords:
Silicon
Electropolishing
Salt film
Potentiodynamic polarization

ABSTRACT

The electropolishing of p-type silicon has been investigated over a wide range of wafer conductivities (p^- to p^{++}) and HF concentrations (0.01–15 wt%) by potentiodynamic polarization. The rate of oxide dissolution was determined from the plateau current density observed in the electropolishing region of the *IV* curve; i.e. where the growth and dissolution rates of the anodic oxide film are equal. The *IV* curves of silicon are reminiscent of a corrosion process control by the dissolution of a salt film in which the rate of reaction is controlled by the removal of dissolved products away from the surface rather than reactants to the surface as previously proposed. For the silicon anodic oxide films this can be by either mass transport or further chemical reaction with HF species in solution. It is shown that this means the dissolution rate should be described by:

$$\text{Dissolution rate} = \frac{DK_{sp}[HF]^2}{\delta} + \frac{k}{A}K_{sp}[HF]^6$$

This relationship is shown to hold for the whole concentration range investigated. Because hydrofluoric acid is a weak acid this rate equation converts to a cubic equation when written in terms of the total HF concentration as opposed to only the HF species, but in this form the connection with the dissolution mechanism is lost.

1. Introduction

Silicon dioxide's excellent dielectric properties mean that it is widely used in the manufacturing of microelectronics. Usually thermal oxides, either grown thermally in dry O_2 or in a wet H_2O vapour atmosphere at temperatures above 900 °C, are used [1]. However thermal oxidation has two main drawbacks; high thermal budget that inevitably leads to a smear-out of steep doping profiles and the restriction that thermal oxide can only be formed on bulk or polysilicon substrates [2]. Alternative methods of oxide formation such as chemical vapour deposition, liquid phase deposition and electrochemical anodization offer the advantage of a lower deposition temperature compared with thermal oxidation [1,2]. Anodic silicon oxides are usually formed in wet etchants based on HF [3].

The microelectronic industry also has a need to remove or thin silicon oxide layers and this is usually achieved by dipping in HF solutions. The high electronegativity of fluoride allows the strong Si—O bond to be broken. As a possible mechanism it has been proposed that the HF molecules react at the silicon surface by adsorption to the lattice Si—O bonds rather than by adsorption to the silicon hydroxyl groups terminating the silicon oxide surface [5]. Several equations are available to describe the dissolution rate of thermal oxides in different electrolytes [6,7]. Nevertheless, these equations tend to be empirical, typically cubic functions of the HF concentration, so provide little insight into reaction mechanisms.

Because the electrical performance of an anodic oxide is inferior to a thermal oxide, device-related applications of anodic SiO_2 are limited to cases where the thermal budget is crucial, e.g. nuclear radiation detectors [4]. As a result of the limited applications, research on the anodic oxide dissolution rates has also been limited compared with that for the dissolution of thermal and CVD formed oxides. Nevertheless, it is generally estimated that the dissolution rates of anodic oxide films are two orders of magnitude larger than the rates for thermal oxides [8–11]. For example, in 1% HF aqueous solutions the dissolution rates for thermal and anodic oxides have been reported to be 3.0 and 300 nm/min (0.05 and 5 nm s^{-1}) respectively [12].

Electrochemical potentiodynamic polarization experiments are an attractive way to study both the growth and dissolution mechanisms of anodic oxide films on silicon. HF does not dissolve bulk silicon at any appreciable rate, therefore within the electrochemical polishing region the anodic oxide dissolution rate should be related to the anodic oxide formation rate, which in turn is given by the anodic current density [9]. That is to say the anodic oxide dissolution rate should be related to the current density in the electropolishing region.

* Corresponding author. Tel.: +65 6516 6289; fax: +65 6776 3604.
E-mail address: msedjb@nus.edu.sg (D.J. Blackwood).

0013-4686/$ – see front matter © 2013 Elsevier Ltd. All rights reserved.
http://dx.doi.org/10.1016/j.electacta.2013.04.024

Table 1
Resistivities and doping densities of the p-type silicon wafers used.

Dopant level (cm^{-3})	Resistivity (Ω cm)
8×10^{19}	0.0015
2×10^{19}	0.004
5.5×10^{17}	0.05
9.5×10^{16}	0.2
3.2×10^{16}	0.5
3.5×10^{15}	4
6.5×10^{14}	10

In this paper, current–voltage (*IV*) curves for p-type silicon in HF are measured over a wide range of both wafer resistivity and electrolyte concentration in order to investigate the relationship between anodic oxide dissolution rate and HF electrolyte concentration. Based on the data obtained a possible mechanism for the rate determining step in the oxide dissolution process is proposed.

2. Experimental

The p-type silicon wafers used were boron doped with (1 0 0) orientation and resistivity ranging from 1.5×10^{-3} Ω cm to 10 Ω cm, as determined via 4-point probe measurements (Table 1). The wafers were cleaved into 1 cm × 1 cm and the native oxide removed in 10 vol% HF, after which GaIn eutectic was applied to the back surface to ensure an Ohmic contact.

The wafers were then mounted as the working electrode in a standard three electrode polytetrafluoroethylene (PTFE) electrochemical cell. The wafers were held vertically in position by clamping with a PTFE washer and O-ring seal that reduced the exposed surface area to 0.017 cm^2. A platinum mesh counter electrode and a saturated calomel reference electrode (SCE), against which all potentials here are reported, completed the cell. The SCE reference electrode was furnished with a polyethylene luggin capillary with the tip positioned at around 5 mm distance from the working electrode to minimize iR drop. The anodizing electrolyte was 0.01–15 wt% HF dissolved in a 1:1 by volume mixture of H_2O and ethanol with the addition of 0.5 M NH_4Cl as a supporting electrolyte; the upper concentration was limited by safety considerations as HF solution above 10 wt% generate considerable amounts of toxic vapour. No external stirring was applied to solutions, i.e. static conditions were maintained. The samples were potentiodynamically polarized at a sweep rate of 5 mV s^{-1} from −300 mV vs. SCE using the potentiostat and sweep generator components of an ACM Instruments field machine. All the *IV* curves presented are after iR compensation. Unless otherwise stated the reported current densities are taken from the forward sweeps and are the average of three runs using fresh wafers each time.

3. Results and discussion

Fig. 1 shows a typical anodic current–voltage curve for moderately doped p-silicon in 3.7 wt% HF electrolyte; the basic shape of the *IV* curves was independent of both HF concentration range (0.01–15 wt%) and wafer resistivity (10^{-3} Ω cm to 10 Ω cm). The *IV* curve can be divided into three potential regions: (i) at the most negative potentials the silicon is under inversion condition so very little current flows in this region; (ii) as the potential is increased the current density starts to rise as a porous silicon layer is formed with a silicon dissolution valence of two; and (iii) at high positive potentials electropolishing occurs, with a dissolution valence of four [8,13]. Within the second region the anodic current initially increases exponentially with applied potential before adopting a linear dependence, as explained elsewhere [12].

The transition from the second to third regions is marked by a peak (usually referred to as j_{ps}) followed by a relatively constant

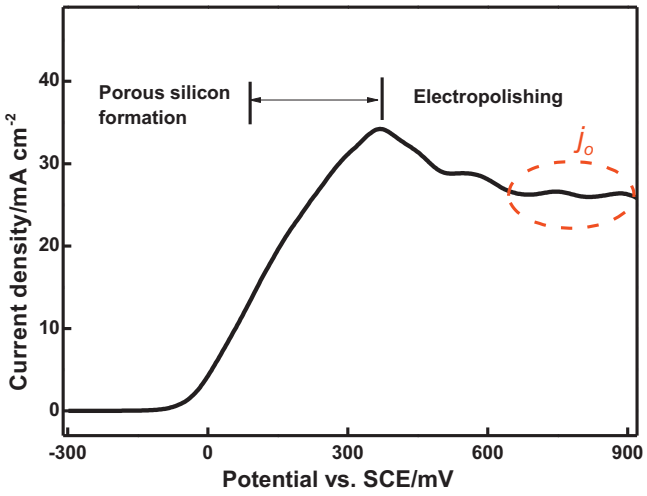

Fig. 1. Typical anodic *I–V* curve measured on a moderately doped (0.05 Ω cm) p-Si wafer in 3.7 wt% HF + 0.5 M NH_4Cl solution.

plateau current density (j_0), a behaviour that is reminiscent of the passivation of metals and alloys [14]. In the case of passivation, the oxide film is very insoluble in the working medium so that the plateau current density arises mainly from thickening of the passive film (along with some capacitance charging). However, in the present case SiO_2 is soluble in HF solutions so the situation is actually closer to the behaviour of the salt films that form during pitting and crevice corrosion [14]. In these cases the corrosion rate is controlled by chemical dissolution of the salt film and steady state conditions are achieved when the rate of corrosion (growth of the salt film) is equal to the film's dissolution rate, such that the observed current density reaches a plateau. That is to say it is believed that the plateau current density in Fig. 1 (marked as j_0) represents the situation where the growth and dissolution rates of the anodic oxide film on the silicon wafer are equal.

At potentials positive of the j_{ps} current peak the silicon's surface is believed to be covered by an oxide that is continuously being dissolved by the HF. The form of the oxide is still unclear with evidence for both a complete film [2] and for closely spaced islands with complete oxide coverage occurring only at the inflection point in the rise of the second electropolishing peak that appears at potentials beyond the positive limit of the present work [15]. The electropolishing process thus occurs in two steps, first the silicon electrode is anodically oxidized and then the oxide is chemically dissolved in the HF [12]. The rate of the oxide growth in the plateau region is directly proportional to the anodic current density [9]:

$$\text{Oxide growth rate} = \frac{j_0 M_w}{nF\rho} \quad (1)$$

where M_w and ρ are the oxides molecular weight (60 g mol^{-1}) and density (2.65 g cm^{-3}) respectively, n is the dissolution valence and F is the Faraday's constant. If the anodic oxide film was SiO_2 then the dissolution valance would be +4, but this is unlikely to be the case for the potential region of the present study where the oxide is believed to be in a hydroxylated form [16,17] and according to the work of Peiner and Schlachetzki [18] the dissolution valance is close to 3.5; this value will thus be used in the present work.

Tables 2 and 3 show the dependencies of the plateau current density and the calculated oxide growth rate, respectively, on HF concentration and wafer resistivity. The standard deviations in j_0 between the three runs under identical conditions were less than 7% of their mean values. It can be seen that both j_0 and the oxide growth rate increase with HF concentration and for the non-degenerate doped wafers are independent of resistivity, which is

Table 2
Influence of HF concentration and silicon wafer resistivity on the plateau current densities (mA cm^{-2}) recorded in the electropolishing region of the *IV* curves.

HF (wt%)	Silicon wafer resistivity (Ω cm)						
	0.001	0.005	0.01	0.2	0.5	3	10
0.01	0.03	0.03	0.03	0.03	0.03	0.03	0.03
0.05	0.10	0.10	0.09	0.09	0.09	0.09	0.09
0.09	0.24	0.24	0.25	0.24	0.23	0.24	0.24
0.13	0.33	0.33	0.36	0.36	0.33	0.34	0.34
0.39	1.67	1.92	2.17	2.22	2.04	2.00	1.97
0.64	3.40	4.43	4.00	5.21	4.90	4.78	5.00
0.90	5.41	6.36	6.75	7.00	7.76	8.02	7.56
1.15	7.57	7.87	8.75	8.35	8.70	9.30	9.04
1.41	10.6	10.4	10.8	13.5	12.7	11.8	12.92
1.66	13.7	14.6	14.1	17.6	15.1	16.0	14.9
1.91	13.6	14.3	16.8	17.5	16.8	17.0	18.5
2.16	15.7	15.7	20.1	19.8	18.9	18.9	20.4
3.79	16.5	20	25.9	25.2	25	25	24
7.45	57	68	85	82	85	90	90
11.0	105	133	160	166	182	187	185
14.4	230	290	447	427	450	439	443

Table 3
Influence of HF concentration and silicon wafer resistivity on the anodic oxide growth/dissolution rate (nm s^{-1}). Dissolution valance is assumed to be 3.5.

HF (wt%)	Silicon wafer resistivity (Ω cm)						
	0.001	0.005	0.01	0.2	0.5	3	10
0.01	0.02	0.02	0.02	0.02	0.02	0.02	0.02
0.05	0.06	0.06	0.06	0.06	0.06	0.06	0.06
0.09	0.16	0.16	0.17	0.16	0.16	0.16	0.16
0.13	0.22	0.22	0.24	0.24	0.22	0.23	0.23
0.39	1.12	1.29	1.45	1.49	1.37	1.34	1.32
0.64	2.28	2.97	2.68	3.50	3.29	3.21	3.35
0.90	3.63	4.26	4.53	4.69	5.20	5.38	5.07
1.15	5.08	5.28	5.87	5.60	5.83	6.24	6.06
1.41	7.12	6.96	7.23	9.07	8.50	7.90	8.66
1.66	9.21	9.81	9.42	11.8	10.1	10.7	9.99
1.91	9.15	9.60	11.3	11.7	11.3	11.4	12.4
2.16	10.5	10.5	13.5	13.3	12.7	12.7	13.7
3.79	11.1	13.4	17.4	16.9	16.8	16.8	16.1
7.45	38.2	45.6	57.0	55.0	57.0	60.3	60.3
11.0	70.4	89.2	107	111	122	125	124
14.4	154	194	300	286	301	294	297

consistent with the previously reported behaviour of j_{ps} [8]. However, for the two highest doped wafers both j_0 and the oxide growth rate decrease with decreasing resistivity. This is consistent with our previous work on the influence of wafer resistivity on j_{ps} in 1 wt% HF diluted electrolyte, where we explained that the lower bias required to oxidize high doped silicon means it is more difficult to break the Si—Si back-bonds thereby favouring electropolishing over porous silicon formation [8].

If the assumption that in the plateau current density region the oxide growth rate is balanced by the oxide dissolution rate is correct, then the rates in Table 3 represent both these parameters. Support for this assumption comes from the work of Nicollian and Brews [9], who determined the dissolution rate of the anodic oxide formed on silicon in 1 wt% aqueous solution to be 5 nm s^{-1}, which is in good agreement with values displayed in Table 3 for p-type silicon in the similar HF concentrations.

It is difficult to envisage why the oxide dissolution rate should be dependent on the wafer's conductivity, so a more likely reason for the apparent lower oxide dissolution rates of the two most conductive wafers is that in these cases the dissolution rate exceeds the growth rate (Fig. 2). That is to say the oxide is completely removed such that there are periods of time where no dissolution is occurring. Indeed, for the two most conductive samples Fig. 2 shows that the current density starts to rise again after a short plateau region towards values concurrent with the more resistive wafers. This is consistent with the additional bias driving the oxide growth at a higher rate, thus the assumption that oxide growth rate is balanced by the oxide dissolution rate in the plateau current density region may not be valid for these degenerate wafers; it being likely that the dissolution rate exceeds the growth rate. Attempts to increase the bias further to ascertain if the most conductive samples would display a second current density plateau close to that of the other wafers were unsuccessful due to the onset of the transition to the second electropolishing peak as described by previous authors [2].

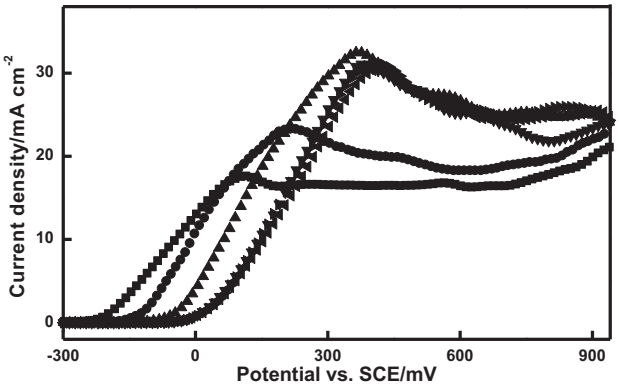

Fig. 2. *I–V* curves for p-type silicon wafers of different resistivities in 3.7 wt% HF + 0.5 M NH_4Cl. ■, 0.0015 Ω cm; ●, 0.004 Ω cm; ▲, 0.05 Ω cm; ▼, 0.2 Ω cm; ►, 0.5 Ω cm; ◄, 4.0 Ω cm; ○, 10 Ω cm. All curves are after compensation for iR drop.

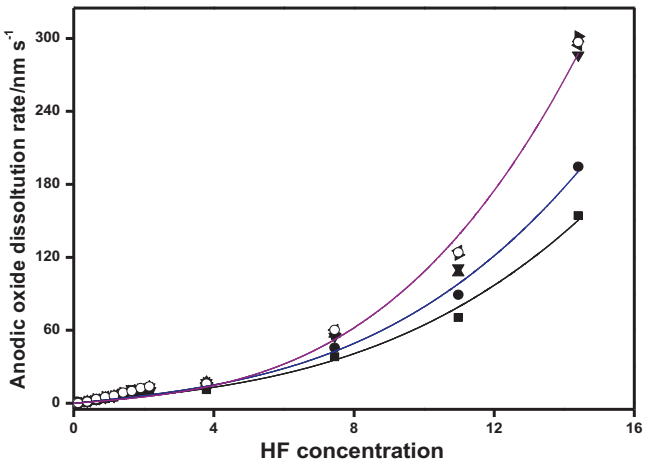

Fig. 3. Dependence of the anodic oxide dissolution rate on HF concentration for differently doped silicon wafers; dashed lines are guides to the eye. ■, 0.0015 Ω cm; ●, 0.004 Ω cm; ▲, 0.05 Ω cm; ▼, 0.2 Ω cm; ►, 0.5 Ω cm; ◄, 4.0 Ω cm; ○, 10 Ω cm.

Fig. 3 shows plots of the oxide dissolution rates against wt% HF for the various doped wafers investigated. It can be seen that at low HF concentrations (<8 wt%) there is an almost linear relationship between the dissolution rate and HF concentration. However, if the HF concentration is further increased the dissolution rate accelerates faster than expected and the linearity is lost. This is not surprising as previous work on thermal oxides has generated empirical relationships between dissolution rate and HF concentration of the form:

$$\text{Dissolution rate} = (A \times c_{HF}) + (B \times c_{HF}^2) + (C \times c_{HF}^3) - D \quad (2)$$

where c_{HF} is in wt% and the constant A is approximately two and three orders of magnitude larger than the constants B and C respectively. For example, data from different authors for thermal oxides are summarized by the equation [2]:

$$\text{Thermal oxide rate}(\text{nm min}^{-1}) = 5.5c_{HF} + 0.047c_{HF}^2 + 0.0065c_{HF}^3 - 2.5 \quad (3)$$

Although it has been demonstrated that the dissolution rate of anodic oxide films are two orders of magnitude faster than their thermal counterparts [1,2,10,11], a similar cubic functions to Eq. (3) can be found to fit the plots in Fig. 3; including the same order of magnitude ratios between the constants A, B and C. Nevertheless, such empirical fits are not very satisfactory and yield little insight into likely reaction mechanisms.

The exact nature of the initial products of the oxide dissolution is unknown, but Kleboth [19] has shown that these can be considered to have the general formula $SiF_i(OH)_j(H_2O)_k$ with $i+j+k=6$. However, because the majority of surface Si atoms can be expected to have two back bonds to bulk O atoms and two hydroxyl terminal bonds the most likely dissolution product is $SiF_2(OH)_2(H_2O)_2$ or simply $SiF_2(OH)_2$, such that the anodic oxide dissolution reaction can be written as:

$$SiO(OH)_{2(s)} + 2HF \leftrightarrow SiF_2(OH)_{2(aq)} + H_2O \quad (4)$$

In reality the reaction is more likely to lead to the rehydration of the oxide than to produce free H_2O, with the whole process being facilitated by hydrogen bonding between the silicon oxide and HF ions as illustrated in (Fig. 4). Note that because the wafers orientation is (1 0 0) a similar mechanism would exist if there is only a monolayer of hydroxide, except that the two back bonds would then be to bulk Si atoms [20].

Virtually all dissolution reactions involve at least two steps, i.e. the actual chemical dissolution step in series with the mass transport of the products from, and/or reactants to, the surface, with the slowest step being rate determining. Therefore in cases where the dissolution is electrochemical in nature the current density (j) flowing will comprise a kinetic (j_k) and diffusion (j_d) component, related by the Koutecky–Levich equation [21–23].

$$\frac{1}{j} = \frac{1}{j_k} + \frac{1}{j_d} \quad (5)$$

In the present case the removal of the initial product of anodic oxide dissolution can occur not only by mass transport but also by further chemical reaction with the HF electrolyte in the immediate in the immediate vicinity of the silicon's surface to produce the known final product H_2SiF_6. Of course this may also occur after the initial product has diffused to the bulk solution but in that case it will not affect the overall oxide dissolution rate:

$$SiF_2(OH)_2 + 4HF \rightarrow H_2SiF_6 + 2H_2O \quad (6)$$

This additional chemical removal route (contributing $j_{k'}$) acts in parallel to the mass transport route but remains in series with the dissolution of the actual oxide film (Reaction (4)), so the Koutecky–Levich relationship becomes:

$$\frac{1}{j} = \frac{1}{j_k} + \frac{1}{j_d + j_{k'}} \quad (7)$$

However, as mentioned above the *IV* curves are reminiscent of a process controlled by chemical dissolution of a salt film, which means the rate limiting step is the removal of soluble products away from the immediate vicinity of the electrode's surface, that is $j_k \gg (j_d + j_{k'})$ in Eq. (7) and Reaction (4) has to be treated as being reversible. Note that a dissolving salt film based mechanism is still consistent with the rotating disc electrode results of earlier workers [2,13–21], who concluded that under static conditions the electropolishing of silicon is mainly limited by the mass transport of fluoride species to the surface, as it only requires a change in interpretation of the direction of movement of the rate controlling species. At high electrode rotation rates, as the mass transport rate increases the assumption that $j_k \gg (j_d + j_{k'})$ would become invalid and the kinetics of oxide growth/dissolution step would start to limit the observed current density. Hence in a Koutecky–Levich plot the intercept at infinite electrode rotation rate has the same meaning, that is $1/(j_k)$, regardless of the whether the mass transport process considered is fluoride to, or dissolution products from, the surface.

With regards to the mass transport of the initial product away from the electrode's surface the use of 0.5 M NH_4Cl supporting electrolyte should mean that the dominate form of mass transport is diffusion across the Nernst diffusion layer for all solutions. Under static conditions Fick's 1st law for simple linear diffusion yields:

$$\text{Flux} = \frac{D(c^{\sigma} - c^{\infty})}{\delta} \quad (8)$$

where D is the diffusion coefficient of the dissolution product, c^{σ} and c^{∞} are the surface and bulk concentrations of the active species and δ is the thickness of the Nernst diffusion layer. For the case of a dissolving salt film c^{σ} represents a saturated solution and is thus much greater than c^{∞}, so Eq. (8) can be simplified to:

$$\text{Flux} = \frac{DC^{\sigma}}{\delta} \quad (9)$$

Although the assumption that the thickness of the Nernst diffusion layer is independent of concentration is not strictly valid the two main parameters that most influence δ are the viscosity and density of the solution, which at room temperature vary by less than 2% and 5% over the range of HF concentrations used, respectively [2,24].

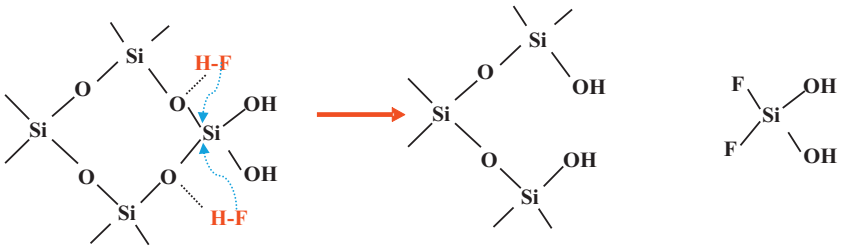

Fig. 4. Schematic illustration of possible anodic oxide dissolution mechanism involving attack by two HF molecules; dotted lines represent hydrogen bonding (Reaction (4)).

Because HF is a weak acid dissociation leads to the presence of HF_2^-, F^-, HF and $(HF)_2$ species according to Eqs. (10)–(12) with equilibrium constants $K_1 = 6.71 \times 10^{-4}$ mol dm^{-3}, $K_2 = 0.259$ mol dm^{-3}, and $K_3 = 0.370$ mol dm^{-3} [2,25].

$$HF \overset{K_1}{\longleftrightarrow} H^+ + F^- \tag{10}$$

$$HF_2^- \overset{K_2}{\longleftrightarrow} HF + F^- \tag{11}$$

$$2HF \overset{K_3}{\longleftrightarrow} (HF)_2 \tag{12}$$

More complex oligomeric fluoride species can exist in concentrated HF with Jones and Penneman [26] reporting infrared spectroscopic evidence that these possibly exist above 6 M (~12 wt%). However, Judge [6] reported that it is unlikely the higher oligomeric species are involved in the dissolution of thermal SiO_2 oxides unless the concentration exceeds 10 M (~21 wt%), therefore these are not considered in the present work.

If it is assumed that the same equilibrium constants apply in EtOH/H_2O mixtures then Table 4 displays the composition of ethanolic HF solutions over the concentration range presently investigated. It is clear that the dominate solutions species are HF and $(HF)_2$, so it is likely that one or both of these are the reactive species. However, since previous studies based on HF + HCl mixtures have suggested that the main active species is undissociated HF [2,27–29], this species will be used for the analysis here.

Under steady state conditions the surface concentration of the initial dissolution will be determined by its rate of generation via oxide dissolution, Reaction (4), and its rate of removal by either mass transport, Eq. (9), or further chemical reaction, Reaction (6):

$$\frac{\partial[SiF_2(OH)_2]^\sigma}{\partial t} = 0 = \left(\frac{\vec{k}}{A}([HF]^\sigma)^2 - \frac{\overleftarrow{k}}{A}[SiF_2(OH)_2]^\sigma\right) - \left(\frac{D[SiF_2(OH)_2]^\sigma}{\delta} + \frac{k'}{A}[SiF_2(OH)_2]^\sigma([HF]^\sigma)^4\right) \tag{13}$$

where $\vec{k}$ and $\overleftarrow{k}$ are the forward and reverse rate constants for Reaction (4), k' is the rate constant for the irreversible Reaction (6) respectively and A is the electrode's surface area.

The anodic oxide dissolution rate is given by the net rate of change in Reaction (4), furthermore because $[SiF_2(OH)_2]^\sigma$ is a saturated solution it can be expressed in terms of its solubility product (K_{sp}) and reactants, assumed here to be HF molecules as depicted in Reaction (4), so Eq. (13) can be rearranged to yield:

$$\text{Dissolution rate} = \left(\frac{D[SiF_2(OH)_2]^\sigma}{\delta} + \frac{k'}{A}[SiF_2(OH)_2]^\sigma([HF]^\sigma)^4\right) = \frac{DK_{sp}[HF]^{2(\sigma)}}{\delta} + \frac{k'}{A}K_{sp}[HF]^{6(\sigma)} \tag{14}$$

where the superscript σ refers to surface concentrations and the dissolution rate has units of mol cm^{-2} s^{-1}. Note that the second term remains as the sixth order of [HF] regardless of the form of the initial $SiF_i(OH)_j(H_2O)_k$ product. Eq. (14) suggests that the dissolution rate should be dominated by mass transport processes at low HF concentrations while chemical reactions become important at high HF concentrations.

Furthermore, because the $(HF)_2$ concentration is second order with HF concentration (Table 4 reveals that $[(HF)_2] = 2.7[HF]^2$ has $R^2 = 1.00$), replacing HF in Reactions (4) and (6) with $(HF)_2$ would only affect the values determined for the parameters K_{sp} and k' in Eq. (14) not the conclusions drawn about the oxide dissolution process. Likewise similar comments apply for the HF_2^- and H^+ ions as their concentrations also scale linearly with that of HF (except for when the total HF <0.1 wt%).

Eqs. (4), (6) and (8) can also be used to define the steady state conditions for the surface concentration of the total HF species:

$$\frac{\partial[c_{HF}]^\sigma}{\partial t} = 0 = \frac{D'([c_{HF}])^\infty - ([c_{HF}])^\sigma}{\delta} - \left(2\left(\frac{\vec{k}}{A}([HF]^\sigma)^2 - \frac{\overleftarrow{k}}{A}[SiF_2(OH)_2]^\sigma\right) + 4\frac{k'}{A}[SiF_2(OH)_2]^\sigma([HF]^\sigma)^4\right) \tag{15}$$

Determining the steady state conditions for the HF molecules at the surface, $\partial[HF]\sigma/\partial t$, is more complicated as the equilibrium Reactions (10)–(12) need to be considered. Nevertheless, substituting Eq. (13) in Eq. (15) and rearranging reveals that the mass transport processes for the HF species and initial dissolution product are in parallel with one another, while being in series with the anodic oxide dissolution kinetic process (a mandatory condition for Reaction (4)).

$$\frac{D'([c_{HF}]^\infty - [c_{HF}]^\sigma)}{\delta} + \frac{4D[SiF_2(OH)_2]^\sigma}{\delta} = 6\left(\frac{\vec{k}}{A}([HF]^\sigma)^2 - \frac{\overleftarrow{k}}{A}[SiF_2(OH)_2]^\sigma\right) \tag{16}$$

Unfortunately Table 4 only shows the bulk concentrations of the possible reactant solution species, whereas Eq. (14) requires knowledge of their surface concentrations. In an electrochemical experiment, under stagnant conditions, the difference between the bulk and surface concentrations when a current density of j_0 is passing can be estimated from [30]:

$$(c^\infty - c^\sigma) = \frac{f_o\delta}{nFD} \tag{17}$$

Assuming that each HF unit, regardless of its species form, supports one electron transfer ($n = 1$) and using a typical value for δ in stagnant aqueous solution of 10^{-2} cm [30] and the reported value for the diffusion coefficient of HF in ethanoic solutions of 2.2×10^{-5} cm^2 s^{-1} [2,23] allows c^σ to be calculated for the range of HF concentrations investigated. Table 5 shows that the c^σ:c^∞ ratio is >90% for all but the three most concentrated solutions, but even in these cases the ratio does not fall below ~70%. Based on these calculations it is not unreasonable to assume that the HF surface concentration is close to its bulk value and as long

Table 4
Concentrations of chemical species present in HF solutions of 0.01–15 wt%.

HF (wt%)	Total HF (c_{HF}) (mol dm^{-3})	[H$^+$] × 10^{-2} (mol dm^{-3})	[F$^-$] × 10^{-4} (mol dm^{-3})	[HF$_2^-$] × 10^{-2} (mol dm^{-3})	[HF] (mol dm^{-3})	[(HF)$_2$] (mol dm^{-3})
0.01	0.00575	0.00165	0.0016	0.00003	0.004	0.00004
0.05	0.0230	0.00355	0.0033	0.00023	0.018	0.0008
0.09	0.0403	0.00475	0.0043	0.00049	0.030	0.0025
0.13	0.0575	0.00570	0.0049	0.00079	0.042	0.0047
0.39	0.173	0.00980	0.0070	0.0028	0.103	0.029
0.64	0.288	0.0126	0.0080	0.0046	0.150	0.060
0.90	0.403	0.0148	0.0086	0.0062	0.189	0.096
1.15	0.518	0.0167	0.0090	0.0077	0.223	0.135
1.41	0.633	0.0184	0.0093	0.0091	0.255	0.175
1.66	0.748	0.0200	0.0095	0.0104	0.283	0.217
1.91	0.863	0.0214	0.0097	0.0116	0.310	0.260
2.16	0.978	0.0227	0.0099	0.0128	0.335	0.303
3.79	1.73	0.0299	0.0106	0.0193	0.472	0.602
7.45	3.45	0.0419	0.0113	0.0306	0.704	1.34
10.98	5.18	0.0511	0.0116	0.0395	0.882	2.10
14.40	6.90	0.0588	0.0118	0.0470	1.03	2.88

as the rate constants for Reactions (10)–(12) are sufficiently fast to maintain their respective equilibrium this will be true for all solutions species. The bulk concentration values in Table 4 can thus be used in place of their surface counterparts in Eq. (14).

Of course there are many potential errors in the calculation used to obtain the c^σ:c^∞ ratios, including:

(i) the value taken for δ is only an order of magnitude estimate, if a larger is taken the calculated c^σ:c^∞ ratios would decline;
(ii) the true value of n is the number of charges required for the dissolution of each silicon atom (most likely 3.5) divided by the number of fluoride atoms in the initial dissolution product, which could vary from two for the $SiF_2(OH)_2$ species shown in Reaction (4) up to six for the final product in bulk solution SiF_6^{2-}, so the true value of n lies between 1.75 and 0.58; and
(iii) the dissolution of the oxide will result in an increase in the local density at the interface, which in the case of the high dissolution rates observed at high HF concentrations could be significantly larger than the bulk density. Because the electrode is vertically aligned the difference in buoyancy between the surface and bulk solutions could cause convective stirring leading to a reduction in the thickness of the diffusion layer and a corresponding increase in the HF c^σ:c^∞ ratios.

Finally note that the validity of Eq. (14) does not depend on having a HF c^σ:c^∞ ratio close to unity as long as this ratio remains reasonably independent of HF concentration it would just behave as a scaling factor in the conversion of $[HF]^\sigma$ to $[HF]^\infty$.

Table 5
Surface (c^σ) to bulk (c^∞) concentration ratios for total HF species calculated from Eq. (17). Assuming n is 1 and typical values for δ and D of 10^{-2} cm and 2.2 × 10^{-5} cm^2 s^{-1} respectively [23,30].

c^∞(mol dm^{-3})	j_0 (mA cm^{-2})	c^σ (mol dm^{-3})	c^σ/c^∞
0.00575	0.03	0.0056	0.98
0.023	0.09	0.0226	0.98
0.04025	0.24	0.0391	0.97
0.0575	0.35	0.0559	0.97
0.1725	2.08	0.163	0.94
0.2875	4.78	0.265	0.92
0.4025	7.42	0.368	0.91
0.5175	8.83	0.476	0.92
0.6325	12.3	0.574	0.91
0.7475	15.5	0.674	0.90
0.8625	17.3	0.781	0.91
0.9775	19.6	0.885	0.91
1.725	25.0	1.61	0.93
3.45	86.4	3.04	0.88
5.175	176	4.35	0.84
6.90	441	4.82	0.70

At low HF concentrations the second term in Eq. (14) can be neglected and Fig. 5 shows plots of the oxide dissolution rates against $[HF]^2$ for the solutions where $c_{HF} < 1$ mol dm^{-3}, revealing linear relationships for all wafer conductivities with an average least mean squared (R^2) value of 0.989. From the average gradient for the five low resistivity wafers (assuming the above values for D and δ of 2.2 × 10^{-5} cm^2 s^{-1} and 0.01 cm) yields a value for K_{sp} of 0.24 dm^3 mol^{-1}. The unusual units for K_{sp} are due to the dependence of the solubility of the anodic oxide on $[HF]^2$ (Reaction (4) and Eq. (14)), i.e. the solubility of the anodic oxide is 0.24 mol dm^{-3} in a solution with [HF] at 1 mol dm^{-3}. Neither [HF] nor $[HF]^3$ provided linear relationships with the oxide dissolution rate, confirming that the main initial product is $SiF_2(OH)_2$ rather than $SiF(OH)_3$ or $SiF_3(OH)$.

According to Eq. (14) the second term (chemical removal of the soluble products from the vicinity of the silicon's surface) should start to make a significant contribution at high HF concentrations. Fig. 6 shows the relationships between the anodic oxide removal rates from the different conductivity wafers and [HF] for the whole concentration range investigated. As predicted from Eq. (14) all the data fit expressions of the form dissolution rate = $A[HF]^2 + B[HF]^6$. Table 6 displays the R^2 values and the required fitting parameters, with the A values having already been determined from the low concentration plots in Fig. 5. According to Eq. (14) the B term should be equal to $k'K_{sp}/A$. Since the solubility product has already been determined from Fig. 5 and the electrode's area is known the values

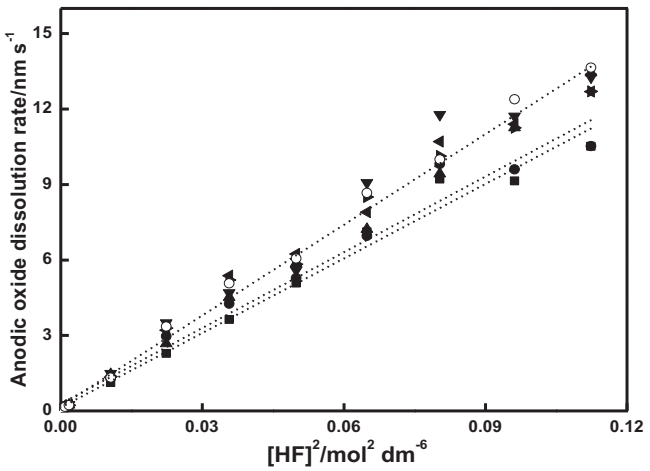

Fig. 5. Dependence of the anodic oxide dissolution rate on $[HF]^2$ for different doped silicon wafers at $c_{HF} < 1$ mol dm^{-3} with best fit linear lines; ■, 0.0015 Ω cm; ●,0.004 Ω cm; ▲, 0.05 Ω cm; ▼, 0.2 Ω cm; ►, 0.5 Ω cm; ◄, 4.0 Ω cm; ○, 10 Ω cm.

Table 6
Fitting parameters required for dissolution rate = $A[HF]^2 + B[HF]^6$ along with R^2 values for fits shown in Figs. 6 and 9. The fitting parameters are displayed for oxide dissolution rates both in units of nm s^{-1} and in units of mol s^{-1}. The A values were obtained from the low [HF] region shown in Fig. 5 or Fig. 8. The data for the far right column was collected on the reverse sweep. From Eq. (14) it can be seen that $A = DK_{sp}/\delta$ and $B = kK_{sp}/A$.

Fitting parameter	Silicon wafer resistivity (Ω cm)							
	0.001	0.005	0.01	0.2	0.5	3	10	0.2 (reverse)
A								
nm s^{-1} dm^6 mol^{-2}	99	100	117	125	117	118	124	71
$\times 10^{-5}$ dm^4 mol^{-1} s^{-1}	4.36	4.41	5.16	5.51	5.16	5.20	5.47	3.12
B								
nm s^{-1} dm^{18} mol^{-6}	32	65	128	112	134	129	124	218.4
$\times 10^{-5}$ dm^{16} mol^{-5} s^{-1}	1.42	2.85	5.65	4.94	5.91	5.69	5.47	9.63
R^2	0.968	0.984	0.970	0.973	0.983	0.988	0.984	0.982

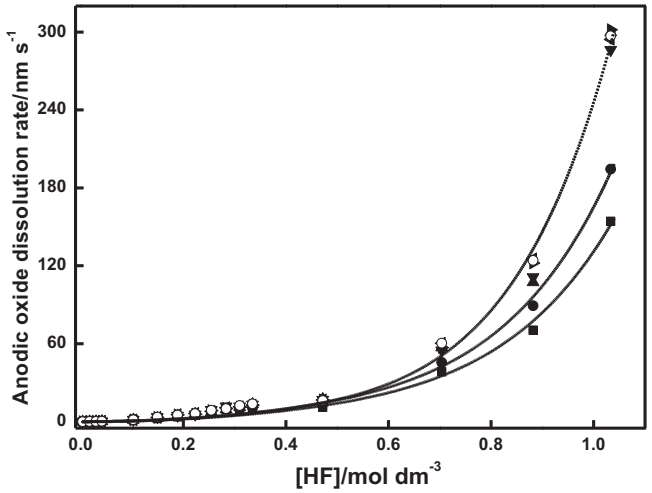

Fig. 6. Dependence of anodic oxide dissolution rate on [HF] for different doped silicon wafers with best fit lines (Eq. (14)); ■, 0.0015 Ω cm; ●, 0.004 Ω cm; ▲, 0.05 Ω cm; ▼, 0.2 Ω cm; ►, 0.5 Ω cm; ◄, 4.0 Ω cm; ○, 10 Ω cm.

in Table 6 can be used to calculate the rate constant for Reaction (6), which for the average of the five most resistive wafers is determined to be 3.9×10^{-8} dm^{15} mol^{-4} s^{-1}.

Up to this point the plateau current densities have been recorded during the forward sweep, but it needs to be recognized that the value of the plateau current density is lower on the reverse sweep; as illustrated in Fig. 7 for the case of a 0.2 Ω cm wafer in 0.12 wt% HF. Table 7 shows that for HF concentrations less than 4 mol dm^{-3} the reverse plateau current densities were on average 80% of their forward counterparts, with a standard deviation of 5%. However, at very high HF levels the difference between the two plateau current densities decreased, being within 3% of one another at the highest HF concentration of 6.9 mol dm^{-3}. The lower reverse plateau current densities mean that the assumption that the current density in j_0 is solely due to anodic oxide growth is not strictly correct, but includes transient contributions associated with the potential sweep rate despite an attempt to minimize these by choosing of a low sweep rate (5 mV s^{-1}). Nevertheless, Figs. 8 and 9 show that the reverse current densities still follow the behaviour expected from Eq. (14), which indicates that the dissolution mechanism proposed in this paper remains valid. Naturally, the lower plateau current densities lead to alternative values of K_{sp} and k' of 0.14 dm^3 mol^{-1} (lower solubility) and 1.2×10^{-8} dm^{15} mol^{-4} s^{-1} respectively (Table 6).

Finally from the data in Table 4 it is found that when the $(HF)_2$ species are taken into account the relationship between c_{HF} and [HF] is quadratic (Fig. 10):

$$c_{HF} = 5.4[HF]^2 + 1.1[HF] \quad (18)$$

Therefore if Eq. (14) is written in terms of c_{HF}, as reported by previous authors, it converts to a cubic equation of the form shown in Eq. (2), although in this form the connection with the dissolution mechanism is lost.

Finally, the assumption that the oxide dissolution rate can be determined from the plateau current density should also be valid in the second electropolishing region at higher potentials where a compact dry oxide, essentially SiO_2, forms [11]. Although current oscillations occur in this region [16,17] the link between the two

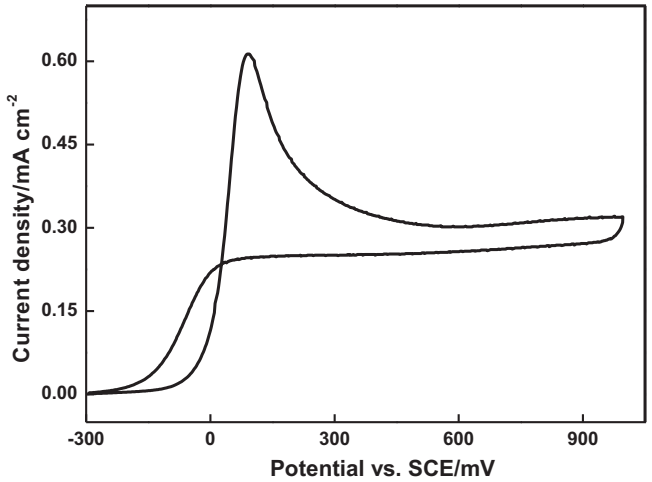

Fig. 7. *IV* curve for 0.2 Ω cm p-type silicon wafer in 0.12 wt% HF showing both forward and reverse scans after compensation for iR drop.

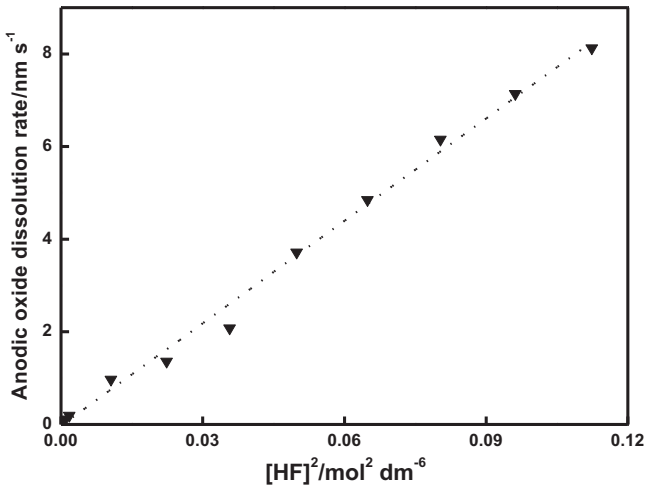

Fig. 8. Dependence of the anodic oxide dissolution rate on $[HF]^2$ for 0.2 Ω cm silicon wafers at $c_{HF} < 1$ mol dm^{-3}. Based on current density plateau in the reverse sweep. R^2 of best fit line is 0.996.

Table 7
Influence of HF concentration on the relative magnitudes of the plateau current densities recorded during the forward and reverse scans for a 0.2 Ω cm p-type silicon wafers.

HF (wt%)	Total HF (c_{HF}) (mol dm^{-3})	j_0 forward (mA cm^{-2})	j_0 reverse (mA cm^{-2})	(j_0 reverse)/(j_0 forward)
0.05	0.0230	0.097	0.081	0.84
0.09	0.0403	0.227	0.169	0.75
0.13	0.0575	0.367	0.286	0.78
0.39	0.173	1.56	1.45	0.93
0.64	0.288	2.58	2.03	0.79
0.90	0.403	3.65	3.10	0.85
1.15	0.518	6.41	5.54	0.86
1.41	0.633	9.47	7.24	0.76
1.66	0.748	11.5	9.2	0.80
1.91	0.863	14.1	10.6	0.75
2.16	0.978	16.3	12.1	0.74
2.67	1.21	18.7	15.4	0.82
3.79	1.73	28.4	22.8	0.80
5.63	2.59	52.6	40.3	0.77
7.45	3.45	81.2	61.8	0.76
9.23	4.31	116	101	0.87
10.98	5.18	206	186	0.90
12.71	6.04	376	361	0.96
14.40	6.90	550	536	0.97

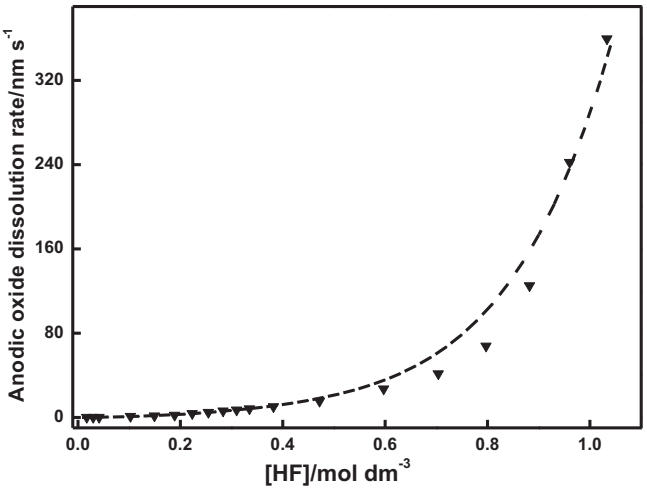

Fig. 9. Dependence of the anodic oxide dissolution rate on [HF] for 0.2 Ω cm silicon wafers. Based on current density plateau in the reverse sweep. R^2 of best fit line is 0.982.

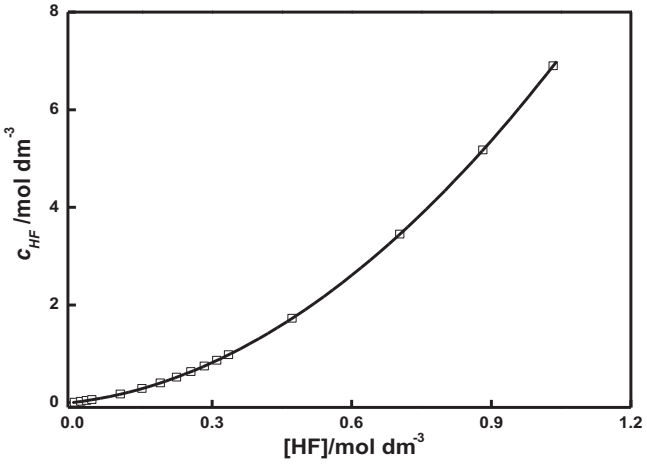

Fig. 10. Quadratic relationship between total HF concentration (c_{HF}) and concentration of molecular HF species [HF] from the data in Table 4.

parameters can be maintained by noting that dissolution depends directly on the available surface area and thus is a function of the oxide roughness.

4. Conclusions

Previous models based on rotating disc electrode experiments have suggested that anodic oxide dissolution is under mixed control, consisting of the kinetics of the oxide dissolution process in series with the mass transport of fluoride ions to the surface with the latter dominating at low rotation rates. However, the *I–V* curves of silicon in ethanolic HF solutions in the first electropolishing region are reminiscent of a corrosion process control by the dissolution of a salt film, in which the rate of reaction is controlled by the removal of dissolved products away from the surface. Therefore in the present work, conducted under stagnant conditions, it is proposed that rather than the movement of fluoride ions to the surface the mass transport component is the movement of the initial soluble products of the oxide's dissolution away from the surface. In this dissolving salt film model it is still expected that the kinetics of the in series oxide dissolution step would start to become rate limiting at high rotation rates, such that the dependency of the measured current density on rotation rate would be the same as that in the previous model based on the movement of fluoride ions.

Recognizing that for the silicon anodic oxide films the removal of the dissolution products from the surface is not solely by mass transport but also by further chemical reaction with HF solution species, and reasoning that the most likely initial dissolution product is either $SiF_2(OH)_2(H_2O)_2$ or simply $SiF_2(OH)_2$, means and that dissolution rate can be described by:

$$\text{Dissolution rate} = \frac{DK_{sp}[HF]^2}{\delta} + \frac{k'}{A}K_{sp}[HF]^6 \quad (19)$$

This relationship was found to hold for the for the whole concentration range investigated (0.01–15 wt%), regardless of whether the plateau current density in the first electropolishing region is recorded from the forward or reverse sweeps of the *IV* curve. The solubility of the initial dissolution product is dependent on the concentration of HF in the electrolyte and for [HF] equal to 1 mol dm^{-3} is found to be either 0.24 or 0.14 mol dm^{-3} if j_0 is taken from the forward or reverse sweeps respectively.

Because there is a quadratic relationship between c_{HF} and [HF], Eq. (19) converts to the cubic equation usually reported by previous authors when written in terms of c_{HF}. However, in this form the

connection with the dissolution mechanism is lost, rendering it a less informative empirical fit.

The main advantages of the new model based on a dissolving salt film is that it is consistent with the j_{ps} peak observed the *IV* curves and, by including the possibility of the soluble product being removed by further chemical reaction with HF solution species as well as by diffusion, it can explain the rapid increase in current density observed at very high fluoride concentrations.

Acknowledgements

Financial support was provided by the NUS-MOE Academic Grant R-284-000-090-112. D.Q.L. acknowledges the support of an NUS scholarship.

References

[1] J. Buhler, F.P. Steiner, H. Baltes, Silicon dioxide sacrificial layer etching in surface micromachining, Journal of Micromechanics and Microengineering 7 (1997) R1–R13.
[2] V. Lehmann, Electrochemistry of Silicon: Instrumentation, Science, Materials and Applications, Wiley-VCH Verlag, Weinheim, 2002, pp. 5–13, 36–38 and 51–96.
[3] D.J. Monk, D.S. Soane, R.T. Howe, A Review of the chemical-reaction mechanism and kinetics for hydrofluoric-acid etching of silicon dioxide for surface micromaching applications, Thin Solid Films 232 (1993) 1–12.
[4] S.A. Campbell, H.J. Lewerenz, Semiconductor Micromachining: Fundamental Electrochemistry and Physics, vol. II, John Wiley & Sons, Chichester, 1998, pp. 263–312.
[5] W.E. Kline, H.S. Fogler, Dissolution of silicate minerals by hydrofluoric-acid, Industrial and Engineering Chemistry Fundamentals 20 (1981) 155–161.
[6] J.S. Judge, Study of dissolution of SiO_2 in acidic fluoride solutions, Journal of the Electrochemical Society 118 (1971) 1772–1777.
[7] S. Verhaverbeke, I. Teerlinck, C. Vinckier, G. Stevens, R. Cartuyvels, M.M. Heyns, The etching mechanisms of SiO_2 in hydrofluoric-acid, Journal of the Electrochemical Society 141 (1994) 2852–2857.
[8] T.L.S.L. Wijesinghe, S.Q. Li, D.J. Blackwood, Influence of doping density on the current–voltage characteristics of p-type silicon in dilute hydrofluoric acid, Journal of Physical Chemistry C 112 (2008) 303–307.
[9] E.H. Nicollian, J.R. Brews, MOS (Metal Oxide Semiconductor) Physics and Technology, Wiley-Interscience, New York, 2002, pp. 741–742.
[10] A. Somashekhar, S. O'Brien, Etching SiO_2 films in aqueous 0.49% HF, Journal of the Electrochemical Society 143 (1996) 2885–2891.
[11] D.J. Monk, D.S. Soane, R.T. Howe, Hydrofluoric-acid etching of silicon dioxide sacrificial layers. 1. Experimental-observations, Journal of the Electrochemical Society 141 (1994) 264–269.
[12] X.G. Zhang, S.D. Collins, R.L. Smith, Porous silicon formation and electropolishing of silicon by anodic polarization in HF solution, Journal of the Electrochemical Society 136 (1989) 1561–1565.
[13] P. Allongue, V. Kieling, H. Gerischer, Etching mechanism and atomic-structure of H—Si (1 1 1) surfaces prepared in NH_4F, Electrochimica Acta 40 (1995) 1353–1360.
[14] G.T. Burstein, Passivity and localized corrosion, in: R.A. Cottis, A. Richardson, R. Lindsay (Eds.), Shreir's Corrosion, vol. 2, 4th ed., Elsevier, Amsterdam, 2010, pp. 731–752 (Chapter 2.02).
[15] G. Hasse, J. Carstensen, G. Popkirov, H. Foll, Current transient analysis of the oxidizing process in the complete anodic regime of the Si–HF system, Materials Science and Engineering B 69–70 (2000) 183–188.
[16] J.N. Chazalviel, M. Etman, F. Ozanam, A voltammetric study of the anodic-dissolution of P—Si in fluoride electrolytes, Journal of Electroanalytical Chemistry 297 (1991) 533–540.
[17] F. Ozanam, J.N. Chazalviel, In-situ infrared characterization of the electrochemical dissolution of silicon in a fluoride electrolyte, Journal of Electron Spectroscopy and Related Phenomena 64–65 (1993) 395–402.
[18] E. Peiner, A. Schlachetzki, Anodic-dissolution during electrochemical carrier-concentration profiling of silicon, Journal of the Electrochemical Society 139 (1992) 552–557.
[19] H.H. Hassan, J.L. Sculfort, M. Etman, F. Ozanam, J.N. Chazalviel, Kinetic and diffusional limitations to the anodic-dissolution of P–Si in fluoride, Journal of Electroanalytical Chemistry 380 (1995) 55–61.
[20] S. Cattarin, I. Frateur, M. Musiani, B. Tribollet, Electrodissolution of p-Si in acidic fluoride media – modeling of the steady state, Journal of the Electrochemical Society 147 (2000) 3277–3282.
[21] J.E.A.M. van den Meerakker, M.R.L. Mellier, Kinetic and diffusional aspects of the dissolution of Si in HF solutions, Journal of the Electrochemical Society 148 (2001) G166–G171.
[22] K. Kleboth, Fluoro complexes of silicon in aqueous solutions, Monatshefte fur Chemie 99 (1968) 1177–1185.
[23] P.J. Hesketh, C. Ju, S. Gowda, E. Zanoria, S. Danyluk, Surface free-energy model of silicon anisotropic etching, Journal of the Electrochemical Society 140 (1993) 1080–1085.
[24] Properties of Hydrofluoric Acid, vol. 1.1, Honeywell Specialty Chemicals, Morristown, NJ, January 2002, pp. 23.
[25] L.J. Warren, Measurement of Ph in acid fluoride solutions and evidence for existence of $(HF)_2$, Analytica Chimica Acta 53 (1971) 199–202.
[26] L. Jones, R. Penneman, Infrared absorption spectra of aqueous HF_2-, DF_2-, and HF, Journal of Chemical Physics 22 (1954) 781–782.
[27] S.A. Campbell, H.J. Lewerenz, Semiconductor Micromachining: Fundamental Electrochemistry and Physics, vol. I, John Wiley & Sons, Chichester, 1998, pp. 282.
[28] C. Serre, S. Barret, R. Herino, Influence of the electrolyte-composition and Ph on the anodic-dissolution of P-type Si in aqueous HF solutions, Journal of Electroanalytical Chemistry 370 (1994) 145–149.
[29] S. Verhaverbeke, H. Bender, M. Meuris, P.W. Mertens, H.F. Schmidt, M.M. Heyns, HF-last cleanings – a study of the properties with respect to the different variables, Materials Research Society Symposium Proceedings 315 (1993) 457–466.
[30] Southampton Electrochemistry Group, Instrumental Methods in Electrochemistry, 2nd ed., Ellis Horwood, Chichester, 1990, pp. 29, 413.